ARTICLE

ACS chemical biology

FMN Binding Site of Yeast NADPH-Cytochrome P450 Reductase Exposed at the Surface Is Highly Specific

Alexis S. Ivanov[†], Oksana V. Gnedenko[†], Andrey A. Molnar[†], Alexander I. Archakov[†], and Larissa M. Podust[‡,*]

[†]Institute of Biomedical Chemistry, Russian Academy of Medical Sciences, Moscow 119121, Russia and [‡]Department of Pharmaceutical Chemistry, University of California, San Francisco, California 94143

ABSTRACT NADPH-cytochrome P450 reductase (CPR) transfers two reducing equivalents derived from NADPH *via* FAD and FMN to microsomal P450 monooxygenases in one-electron transfer steps. The crystal structure of yeast CPR (yCPR) contains a surface-exposed FMN binding site (FMN2 site) at the interface of the FMN binding and connecting domains, in addition to the single buried site that has been observed in rat CPR. This finding provides a testable hypothesis of how intramolecular (between FAD and FMN) and intermolecular (between FMN and P450) electron transfer may occur in CPR. To verify that occupancy of the FMN2 site is not an artifact of crystallization, a surface plasmon resonance (SPR) biosensor technique has been applied to probe the selectivity of this site under functional conditions. A series of kinetic and equilibrium binding experiments involving yCPR immobilized on different sensor chip surfaces was performed using FMN and FAD, as well as FMN-derived compounds, including riboflavin, dimethylalloxazine, and alloxazine, and other molecules that resemble the planar isoalloxazine ring structure. Only FMN and FAD showed stoichiometric binding responses. Binding affinity for FMN was in the submicromolar range, 30 times higher than that for FAD. Association kinetic rates for the yCPR/FMN complex were up to 60-fold higher than for the yCPR/FAD complex. Taken together, these data indicate that (i) the surface-exposed site in yCPR is highly selective toward binding flavins, (ii) binding of FMN in this site is notably favored, and finally, (iii) both the phosphate group and the isoalloxazine ring of FMN are essential for binding.

NADPH-cytochrome P450 reductases (CPRs) belong to a family of diflavin-containing electron transport proteins that transfer a hydride ion from NADPH and channel the two reducing equivalents derived from the hydride ion *via* the FAD and FMN prosthetic groups in one-electron transfer steps to structurally diverse proteins including the large superfamily of microsomal P450 monooxygenases (P450, CYP), squalene monooxygenase (*1, 2*), heme oxygenase (*3*), fatty acid desaturase (*4*), and cytochrome b_5 (*5*). The family of diflavin electron transporters also includes the *Bacillus megaterium* cytochrome $P450_{BM3}$ reductase (*6*) and structurally related homologues from *Bacillus subtilis* (*7*) and *Fusarium oxysporum* (*8*), as well as nitric oxide synthase (*9*), methionine synthase reductase (*10*), novel reductase 1 (*11*), and the α subunit of bacterial sulfite reductases (*12*). The mechanism of electron transfer between CPR and P450 has still not been established after more than four decades of intense research and remains both elusive and controversial despite extensive studies using kinetic, spectroscopic, crystallographic, and site-directed mutagenesis techniques (*13–16*).

Separate lines of research converge on the involvement of intramolecular conformational changes to the reductase during electron transfer to P450 enzymes. One line of investigation supports CPR protein domain dissociation (*17–19*), while another one points to a flipping of the FMN cofactor between two binding sites within CPR (*20*). In the latter hypothesis CPR obtains electrons from FAD at one site and delivers them to the P450 electron acceptor at the other. This hypothesis is based on the crystal structure of fully functional yeast

*Correspondoing author, larissa.podust@ucsf.edu.

Received for review March 9, 2010 and accepted June 16, 2010.

Published online June 17, 2010

10.1021/cb100055v

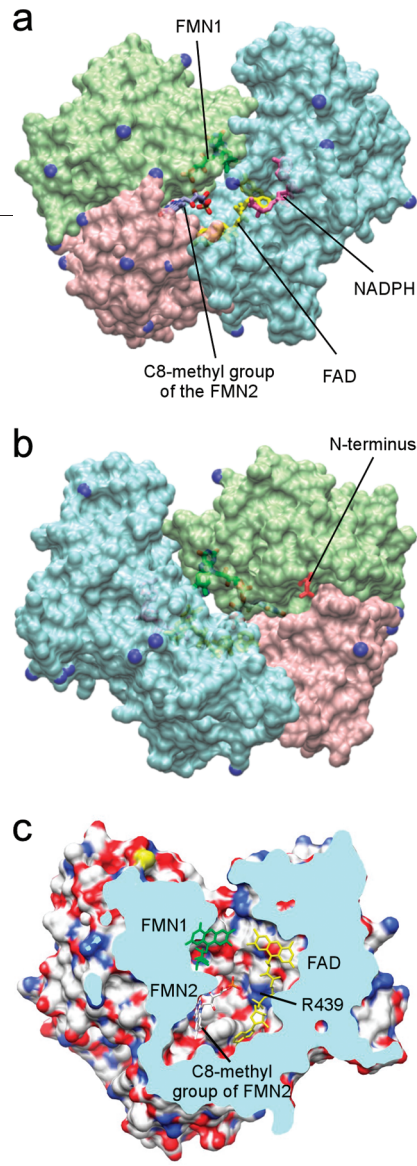

Figure 1. yCPR domain structure and cofactor binding. Front (a) and back (b) views of yCPR represented by semitransparent surfaces of the FMN binding (light green), FAD/NADPH binding (cyan), and connecting (rose) domains. Amino groups of lysine residues accessible for immobilization on the CM5 surface are shown by the blue nitrogen van der Waals spheres. a) FMN2 is clearly visible in the front view through the opening between yCPR domains. NADPH is highlighted in magenta, FAD in yellow, FMN1 in green, and FMN2 in blue. Oxygen atoms of FMN are in red, phosphorus in yellow-green. b) The image is rotated ~180° around the vertical axis in the plane of the drawing compared to the image in panel a. The first visible N-terminal residue, N47, in the yCPR structure to which a sequence carrying a His_{12} tag is attached, is shown in red. Images were prepared using VMD software (*42*). c) View of yCPR clipped by the plane (cyan) through the cofactor-binding bowl. Surface and FMN2 are colored by elements, FMN1 is green, FAD is yellow. NADPH is removed for clarity. Image was prepared using CHIMERA (*43*).

CPR (yCPR) (*20*), which revealed a novel, to our knowledge, second FMN-binding site at the interface of the FMN binding and connecting domains (Figure 1) in addition to the FMN binding site (FMN1 site) observed previously in rat CPR (*21*). Activity of the yCPR does not require added FMN; thus if the FMN2 site is involved in electron transport, it is likely that a single FMN moves between the two sites. The dimethylbenzene edge of the FMN2 isoalloxazine (specifically the C8-methyl group) protrudes from below the protein surface toward two nearby acidic clusters that were mapped to bind cytochrome *c* and P450 (*22–24*).

In contrast, current structural knowledge of mammalian CPR has been based until recently on the X-ray structure of a compact conformation of the truncated rat CPR lacking the 64 N-terminal residues (*21, 25*), which can reduce cytochrome *c*, a nonphysiologic substrate, but is inactive toward microsomal cytochromes P450, its physiological partners (*26, 27*). From the compact CPR structure it is difficult to rationalize how a large electron acceptor such as P450 could approach sufficiently closely to the FMN1 isoalloxazine ring for electron transfer to occur. More recently, the crystal structures of the engineered human CPR with the truncated hinge connecting the FMN binding domain to the rest of the molecule (*18*) or with the FMN domain swapped with its yeast counterpart (*17*) have been determined in extended conformations, with the FMN domain virtually dissociated from the rest of the CPR molecule. Also, the combined NMR and small-angle X-ray scattering (SAXS) studies predict two-state equilibrium between the compact and extended human CPR conformations in order to satisfactorily describe the shape of the experimental scattering profile (*19*). All three research groups hypothesize that to accept electrons a P450 enzyme would bind to the dissociated FMN binding domain.

An alternative structure-based mechanism implicating flipping of the FMN cofactor between two binding sites within enclosed protein environment rather than domain dissociation has been proposed in our prior work (*20*). The proposed mechanism is consistent with the P450 requirement of two one-electron donation steps separated in time and with experimental observations that CPR from the different species differ in their FAD and FMN environments, redox potentials, and kinetic parameters (*13*). Residues constituting the FMN2 site are far less conserved across the *cpr* gene family but clearly show phylum-specific variations that may modulate the redox characteristics of different CPRs (*20*). Consistent with the FMN flipping hypothesis is the well documented phenomenon that FMN, in contrast to FAD, can be reversibly released from mammalian CPR *in*

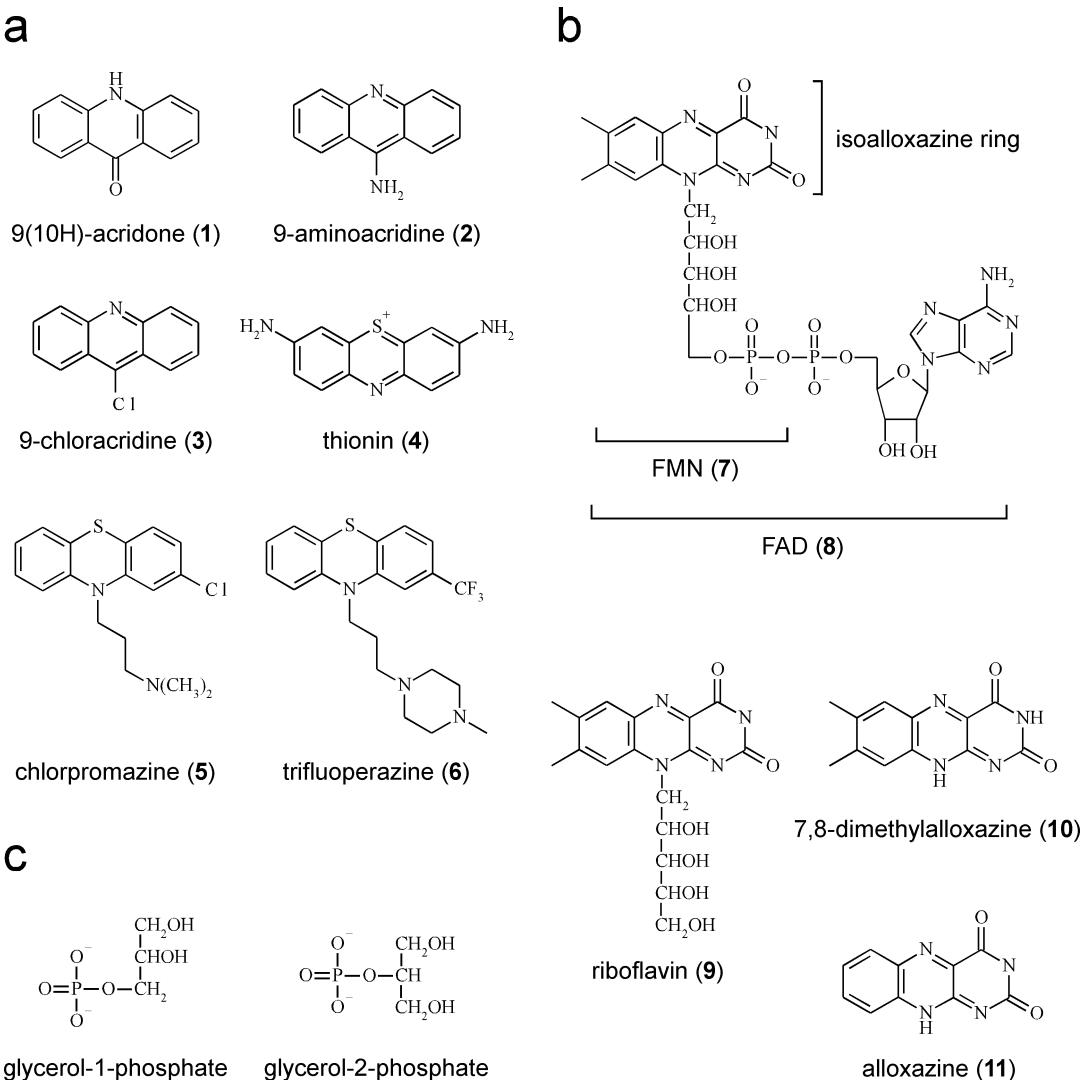

Figure 2. Organic molecules used for probing the yCPR FMN2 binding site. a) Chemical structures of small organic molecules selected based on similarity of their chemical structures to isoalloxazine ring system. b) FMN, FAD, and FMN-derived molecules lacking a phosphate group. c) Glycerol phosphates.

vitro, whereas to release FAD, CPR must be partially denatured (*28, 29*). Detection of a unique second FMN binding site in an essential and extensively studied electron donor protein such as CPR was a surprising discovery, and we were alert to the possibility that the observation might be an artifact of crystallization. Accordingly, in the present work we applied surface plasmon resonance (SPR) biosensor technology (*30*) to address selectivity of the yCPR FMN2 site under native functional conditions and to ascertain if occupancy of this site in the crystal was due to salting-in of an organic molecule into a random hydrophobic pocket or to unspecific interactions *via* a phosphate group. We have developed a system employing yCPR attached to the surfaces of different biosensor chips to examine binding of FMN, FAD, as well as derivatives of FMN, and a number of low molecular weight organic compounds resembling the planar structure of the isoalloxazine ring (Figure 2). These experiments revealed a surface-exposed site that is highly selective toward binding flavin prosthetic groups,

FMN and FAD, and that FMN binds in this site with a submicromolar K_D, at least an order of magnitude tighter than that of FAD. Kinetic rate association constants (k_{on}) for the yCPR/FMN complex obtained on two different surfaces are 40- to 60-fold greater than those of the yCPR/FAD complex. Neither inorganic phosphates nor glycerol phosphates in the running buffer affected FMN or FAD binding in the FMN2 site, indicating that binding is specific and requires the simultaneous presence of both the phosphate group and izoalloxazine ring.

RESULTS AND DISCUSSION

Immobilization of yCPR on Sensor Chip Surfaces. The yCPR was immobilized either on an NTA chip *via* the His_{12} tag or, alternatively, on a CM5 chip by covalent coupling *via* protein lysyl amino groups. The amount of yCPR immobilized on the Ni-NTA chip was optimal with 3 ng per flow cell (Figure 3, panel a), maximizing the response signal and at the same time minimizing baseline drift due to dissociation of weakly bound protein molecules. The NTA sensor surface has a relatively low binding capacity. At higher immobilization levels not all protein molecules have full access to the Ni-NTA sites for efficient binding, and thus higher dissociation rates are observed. Drift of the biosensor signal creates considerable problems for analysis of small molecule binding to immobilized protein, although correction of systematic baseline drift using an algorithm implemented in Biacore Evaluation Software (GE Healthcare) allowed the concentration dependence of the equilibrium signal for FMN and FAD binding to yCPR to be obtained.

Covalent coupling of the target protein to the CM5 surface overcomes the signal drift problem and allows a higher amount of immobilized protein (Figure 3, panel b). However, covalent attachment *via* solvent-accessible lysine residues is random and results in many possible permutations of the conjugation pattern, including those leading to protein orientations on the chip that are unproductive for further ligand binding.

Binding of Flavin Cofactors to yCPR. The fact that the biosensor response is directly proportional to the amount of immobilized material leads to the conclusion that Ni-NTA immobilized yCPR binds FMN with 1:1 stoichiometry at saturating concentrations of FMN. In this regard, the value of yCPR saturation response on the Ni-NTA surface (3000 RU) divided by the protein/ligand molecular weight ratio ($77{,}000_{yCPR}/460_{FMN} = 167$ or $77{,}000_{yCPR}/830_{FAD} = 93$) results in a maximal signal increase value (18 RU for FMN and 32 RU for FAD) for 1:1 yCPR/ligand binding stoichiometry. Indeed, the FMN binding response on the Ni-NTA surface at saturating concentrations is within 18 RU difference between the sample and reference channels (Figure 4, panel a), indicating that all yCPR molecules on the surface are bound to FMN. At the same time, the FAD response is within 25 RU (Figure 4, panel b), which is lower than the potential maximum for equimolar binding, indicating that about 75% of the immobilized yCPR molecules are bound to FAD. Accordingly, the yCPR saturation response on the CM5 surface (12,000 RU) divided by the protein/ligand molecular weight ratio would result in maximal signal increase values of 72 RU for FMN and 129 RU for FAD for 1:1 binding stoichiometry. In prac-

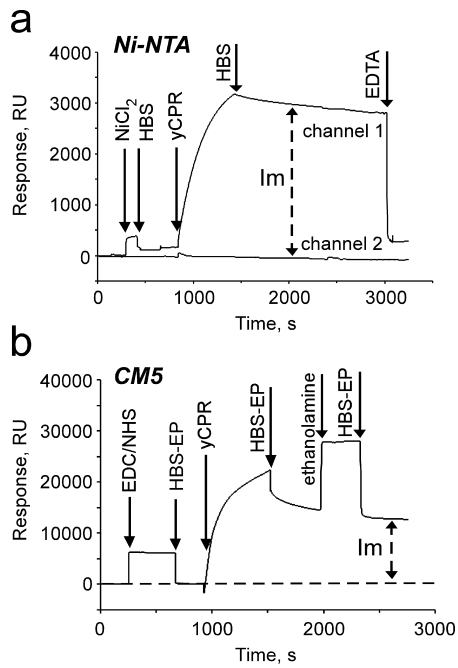

Figure 3. Sensograms of yCPR immobilization on Biacore chips. a) yCPR immobilization on Ni-NTA chip. Channel 1: activated Ni-NTA surface. Channel 2: nonactivated NTA surface. HBS, NTA chip running buffer; yCPR, 100 nM yCPR in HBS running buffer; EDTA, NTA chip regeneration solution. b) yCPR immobilization on CM5 chip. EDC/NHS, CM5 surface activation solution; HBS-EP, CM5 chip running buffer; yCPR, 0.65 μM yCPR in 10 mM acetate buffer, pH 5.5; ethanolamine, 1 M ethanolamine, pH 8.5. Im = quantity of immobilized yCPR in RU (1 RU = 1 pg of protein).

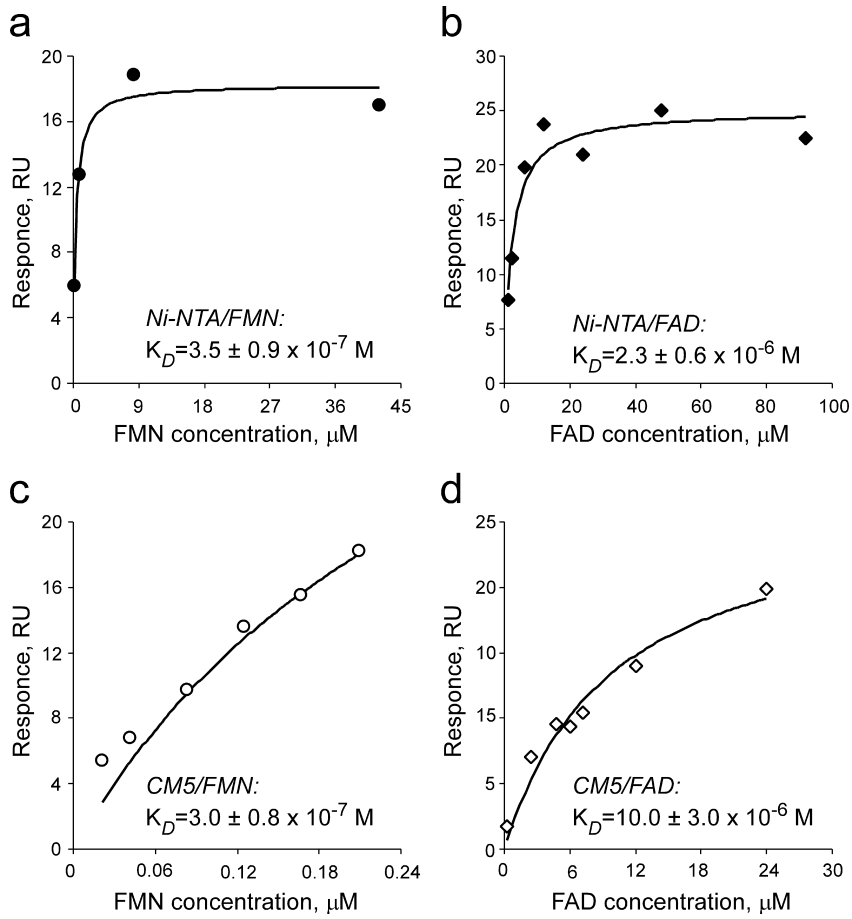

Figure 4. Equilibrium data analysis of FMN and FAD binding to yCPR. Dependence of NTA (a, b) and CM5 immobilized yCPR (c, d) equilibrium signal on FMN or FAD concentrations. The data for the SPR sensorgrams were fitted to a single-site interaction model. Individual curves for one series of measurements are shown in each panel. Each series of measurements was repeated at least five times and reported in Table 1 as the average of five independent determinations.

tice, the FMN response at saturating concentrations is within 22 RU (Figure 5), indicating that less than one-third of immobilized yCPR molecules are bound to FMN. Therefore, more than two-thirds of the yCPR molecules are apparently immobilized on the CM5 chip in orientations unproductive for ligand binding. This ratio agrees with the distribution of 22 solvent-accessible lysines on the yCPR surface, a majority of which are concentrated around the opening between the yCPR domains, which apparently serve to provide access for FMN to the FMN2 site (Figure 1, panel a). By contrast, the His_{12} tag is located on the opposite yCPR surface (Figure 1, panel b), defining a single attachment point to achieve a more specifically oriented layer where all molecules are accessible for ligand binding.

Analysis of yCPR/flavin stoichiometry performed previously (*20*) indicates that yCPR retains a single copy of each flavin acquired during *E. coli* expression through all purification steps, which agrees with the properties of rat CPR, where reversible FMN removal can be achieved only upon treatment with 2 M KBr at slightly alkaline pH over 12−14 h (*31*). To exclude any possibility of FMN depletion during the inactivation of residual active groups on the CM5 surface, treatment of the chip surface with ethanolamine was substituted with several hours of continuous washing with the HBS-EP buffer that

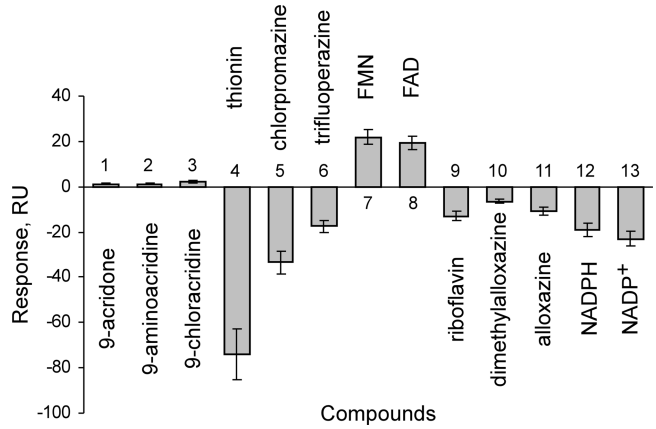

Figure 5. Ligand binding to yCPR immobilized on the CM5 chip. Compound numbering is the same as in Figure 2. The biosensor response corresponds to the difference of equilibrium signals between sample (+yCPR) and reference (−yCPR) channels. Compound concentrations were within a 25−30 μM range. Nonspecific interactions of compounds with the dextran matrix in the reference channel result in a negative difference signal. Each measurement was repeated at least four times.

lead to spontaneous inactivation of the reactive groups. These changes in the immobilization protocol did not affect FMN or FAD binding (data not shown), indicating that the same number of binding sites is available for binding under both inactivation conditions, showing that the immobilization procedures did not result in cofactor depletion. To the contrary, an attempt to remove FMN from the FMN1 site by continuous wash of yCPR immobilized on the CM5 chip with 2 M KBr solution resulted in the irreversible loss of yCPR's ability to bind either FMN or FAD, probably because of protein denaturation.

Binding of Organic Molecules to yCPR. Yeast CPR immobilized on the CM5 surface of the sensor chip was probed with the flavin prosthetic groups FMN and FAD, as well as with truncated FMN-derived molecules such as riboflavin, dimethylalloxazine, and alloxazine (Figure 2, panel b) and a number of low molecular weight compounds selected for their resemblance to the planar structure of the isoalloxazine ring (Figure 2, panel a). NADPH and NADH were also used to probe the solvent-exposed NADPH binding site on the CPR surface. Small positive responses were generated by the acridine derivatives, compounds **1**−**3**. Although none of the compounds **4**−**6** and **9**−**13** generated a positive response upon addition to immobilized yCPR, they interacted nonspecifically with the dextran surface, which resulted in a negative difference signal between sample and reference channel due to the larger accessible dextran surface in the reference channel (Figure 5). These compounds included chlorpromazine (**5**) and trifluoperazine (**6**), commonly used antipsychotic tranquillizers shown elsewhere to inhibit NADPH-induced microsomal lipid peroxidation in rats by inhibiting CPR (*32*). However, neither compound generated a positive response, indicating that no SPR-detectable binding occurred with yCPR. A significant finding was that a series of flavin-derived molecules lacking a phosphate group, *e.g.*, riboflavin (**9**), 7,8-dimethylalloxazine (**10**), and alloxazine (**11**) (Figure 2, panel b), also did not show positive binding, indicating an essential role for the phosphate group. No positive binding was detected for NADPH and $NADP^+$ (**12**, **13**), perhaps due to the solvent-accessible nature of the NADPH binding site in CPR that may result in high k_{on} and k_{off} values for the CPR−NADPH complex. These data confirm that the FAD binding observed by Biocore occurs through its FMN moiety and that the adenosine diphosphate moiety does not contribute to binding. In contrast, FMN (**7**) and

TABLE 1. Kinetic and thermodynamic parameters of FMN and FAD binding to immobilized yCPR[a]

Complex	Chip surface	k_{on}, M^{-1} s^{-1}	k_{off}, s^{-1}	K_D (k_{off} /k_{on}), M (calculated)	χ^2	K_D, M (steady state)	χ^2
yCPR/FMN	NTA	$(5.8 \pm 0.5) \times 10^4$	$(9.5 \pm 0.6) \times 10^{-3}$	$(1.6 \pm 0.2) \times 10^{-7}$	6.79	$(3.5 \pm 0.9) \times 10^{-7}$	1.43
	CM5	$(8.4 \pm 0.1) \times 10^4$	$(9.95 \pm 0.07) \times 10^{-3}$	$(1.18 \pm 0.02) \times 10^{-7}$	0.145	$(3.0 \pm 0.8) \times 10^{-7}$	2.26
yCPR/FAD	NTA	$(1.39 \pm 0.02) \times 10^3$	$(5.0 \pm 0.1) \times 10^{-3}$	$(3.60 \pm 0.09) \times 10^{-6}$	2.22	$(2.3 \pm 0.6) \times 10^{-6}$	4.22
	CM5	$(1.36 \pm 0.03) \times 10^3$	$(6.04 \pm 0.08) \times 10^{-3}$	$(4.4 \pm 0.1) \times 10^{-6}$	0.304	$(10 \pm 3) \times 10^{-6}$	1.51

[a] k_{on} = association rate constant; k_{off} = dissociation rate constant; K_D = equilibrium dissociation constant. $\chi^2 = \Sigma(r_{fi} - r_{xi})^2/(n - p)$, where r_{fi} is a fitted value at the ith point, r_{xi} is an experimental value at the same point, n is the number of data points, and p is the number of fitted parameters. All data reported are the average of five independent determinations

FAD (**8**) generated clear stoichiometric (FMN) or substoichiometric (FAD) responses, which we interpreted as binding of flavin cofactors to the surface-exposed site of yCPR immobilized on the chip surface, likely the same one observed in the X-ray structure of yCPR (*20*).

Although the FMN phosphate group does not make direct salt-bridge interactions in the FMN2 sites (*20*), electrostatic interactions are suggested with Arg439, which is within 5.8 Å from the FMN2 phosphate (Figure 1, panel c). An invariant residue across the *cpr* gene family, Arg439 makes salt-bridge contacts with both the FAD diphosphate moiety and Glu361. These interactions are apparently indispensable for CPR function, as the negative charge at Glu361 is conserved in CPR *via* phylum-specific replacement with an aspartate. Electrostatic interactions with Arg439 may synergize with the H-bonding interactions between the FMN2 ribityl moiety and Asp187, making the FMN ribitylphosphate tail indispensable for binding. When the FMN2 site is occupied during the electron transfer and thus when the FMN1 site is empty, some conformational changes might occur to generate additional FMN contacts in the FMN2 site.

Kinetic and Thermodynamic Parameters of FMN and FAD Binding to yCPR. The equilibrium K_D values for FMN and FAD binding to yCPR immobilized either on Ni-NTA or CM5 surfaces have been calculated from the dependence of the equilibrium binding signal on ligand concentration (Figure 4 and Table 1). K_D values of $(3.5 \pm 0.9) \times 10^{-7}$ and $(2.3 \pm 0.6) \times 10^{-6}$ M were obtained for the yCPR/FMN and yCPR/FAD complexes, respectively, on the Ni-NTA surface. These differences in equilibrium dissociation constants indicate that the yCPR/FMN complex is >6 times tighter than the yCPR/FAD complex. On the CM5 surface, steady-state binding experiments resulted in a very similar K_D value of $(3.0 \pm 0.8) \times 10^{-7}$ M for the yCPR/FMN complex and a 4-fold higher K_D value of $(10.0 \pm 3.0) \times 10^{-6}$ M for the yCPR/FAD complex, suggesting that the yCPR/FMN complex is 30 times tighter. Kinetic rate constants were calculated from corresponding kinetic curves measured at different ligand concentrations (Table 1). Bimolecular association rate constants, k_{on}, for the yCPR/FMN complex are consistently 40−60 times higher than those for the yCPR/FAD complex on both Ni-NTA and CM5 surfaces. Thermodynamic constants calculated using kinetic rates indicate binding affinity for the yCPR/FMN complex 20−40 times higher than for yCPR/FAD, depending on the surface type. Apparently, kinetic and steady-state results agree better on the CM5 surface, probably due to higher experimental error associated with the baseline drift on the Ni-NTA chip.

K_D values determined for complexes with both FMN and FAD suggest that binding of FMN in the FMN2 site is notably favored. FAD, with an adenosine moiety attached through a pyrophosphate group, is perhaps too bulky to be unambiguously and rapidly positioned in the FMN2 site, consistent with its significantly reduced association rate and binding affinity. Association kinetic rates (k_{on}) obtained for both yCPR/FMN and yCPR/FAD complexes are considerably lower than in diffusion-controlled binding. This may be due at least in part to the relatively buried nature of the FMN2 site (Figure 1), which results in a diffusion barrier hampering FMN access from the bulk solvent. However, these values do not pertain to the putative mechanism of FMN shuttling that is predicted to occur without dissociation of FMN from the reductase upon entry to the FMN2 site from the protein interior.

Role of a Phosphate Group in FMN Anchoring. The specific binding of phospholipids to CPR has been demonstrated previously (*33*–*36*). The major effect of phospholipids on P450 enzymatic activities is attributed to their facilitation of the formation of an active P450/CPR complex (*37*). A series of control experiments on FMN and FAD binding in the presence of orthophosphate, pyrophosphate, or glycerol phosphates (at 1 mM concentration in the running buffer) was performed to find out if phosphate-containing metabolites compete with FMN or FAD for binding in the FMN2 site. We found that none of these metabolites, including glycerol-1-phosphate (comparable to FMN but lacking an isoalloxazine ring and a carbinol module (Figure 2, panel c)), affected FMN or FAD binding in the FMN2 site (data not shown). This result rules out the possibility that FMN binding occurs in a random protein pocket with accidental affinity to the phosphate anion, indicating that the FMN2 site can function in the phosphate-rich environment of living cells (*e.g.*, the orthophosphate level in yeast cells exceeds 20 mM (*38*)). Lack of competition with glycerol-1-phosphate indicates also that the isoalloxazine ring is a prerequisite of specific FMN binding in the FMN2 site.

In summary, the concept of flavin motion as integral to catalytic function has been developed for *p*-hydroxybenzoate hydroxylase and related flavopro-

teins that catalyze hydroxylation of an aromatic ring (*39*). In these enzymes, movement of flavin occurs by rotation of the isoalloxazine ring about the ribityl side chain in the plane of the ring and is coupled with the reduction by NADPH followed by reaction with oxygen to form a flavin-C4-hydroperoxide, an active form of oxygen in flavoprotein hydroxylases. A similar FMN flipping mechanism has been suggested by the X-ray structure of yeast CPR (*20*) as opposed to an alternative domain dissociation hypothesis that prevails for human CPR (*17–19*) and nitric oxide synthase (*40*). Given that FMN delivers one electron at a time, the FMN-domain-P450 complex would have to disassemble after the delivery of the first electron in order to allow FMN to reassociate with FAD to obtain the second electron. Although such a domain "flapping" is feasible in principle, the flapping rate must be fast enough to accommodate measured FMN-FAD electron transfer rates as well as the much slower rates of P450 catalysis. Because FMN flipping is unencumbered by domain dissociation/association, it would occur on a faster time scale. Further, the observations that intramolecular electron transfer from FAD to FMN is completely or essentially impaired in CPR variants engineered to adopt an extended conformation (*17–19*) are not in favor of domain flapping hypothesis. In any case, a CPR system competent in physiological electron transfer to P450 should be a starting point to invalidate one or the other hypotheses.

METHODS

Protein Preparation. The truncated form of yCPR lacking 33 residues, including the N-terminal hydrophobic membrane anchor (*41*), which has been successfully used in crystallographic studies (*20*), was further modified by extension of the N-terminal His tag from 6 to 12 His residues to enhance its immobilization on the Ni-NTA chip of the biosensor instrument. The protein was expressed and purified as described previously (*20*).

Chemicals and Consumables. Low molecular weight organic compounds 9(10*H*)-acridone (*1*), 9-chloroacridine (*3*), and 7,8-dimethylalloxazine (*10*) were purchased from Acros Organics; 9-aminoacridine hydrochloride (*2*) and thionin (*4*), from Alfa Aesar; chlorpromazine (*5*), trifluoperazine dihydrochloride (*6*), FMN (*7*), FAD (*8*), riboflavin (*9*), alloxazine (*11*), NADPH, and $NADP^+$ from Sigma-Aldrich. Glycerol phosphates and inorganic phosphates were purchased from Fluka. The structures of compounds are shown in Figure 2.

For binding experiments, all compounds were dissolved in DMSO as 1 mM stock solutions. These stock solutions were diluted with running buffer to the working concentrations ranging from 25 to 30 μM, which reduced the DMSO concentration to ~3% (v/v). For experiments on yCPR/FMN and yCPR/FAD complexes dilution of corresponding stock solutions was in the 20 nM to 45 μM range.

HBS (NTA chip running buffer) (10 mM HEPES, pH 7.4, 150 mM NaCl, 0.05 mM EDTA, 0.005% surfactant P20), NTA chip regeneration solution (10 mM HEPES, pH 8.3, 150 mM NaCl, 350 mM EDTA, 0.005% surfactant P20), HBS-EP (CM5 chip running buffer) (10 mM HEPES, pH 7.4, 150 mM NaCl, 3 mM EDTA, 0.005% surfactant P20), amine coupling kit, 1-ethyl-3(3-dimethylaminopropyl)-carbodiimide hydrochloride (EDC), *N*-hydroxysuccinimide (NHS), ethanolamine-HCl, research grade sensor CM5 chips carrying hydrophilic carboxymethylated dextran matrix, and sensor NTA chips carrying carboxymethylated dextran preimmobilized with chelating agent nitrilotriacetic acid were all purchased from GE Healthcare (USA).

Immobilization of yCPR on NTA Sensor Chip Surface. The yCPR was immobilized on an NTA chip *via* the His_{12} tag. The sensor surface (with preimmobilized NTA chelating agent) was activated by injection of 0.5 mM $NiCl_2$ in HBS running buffer at a flow rate of 10 μL min^{-1} to saturate NTA sites, followed by washing with HBS buffer alone (Figure 3A). Then 100 nM His_{12}-tagged yCPR in HBS buffer was injected at a flow rate of 10 μL min^{-1} until the baseline level stabilized at ~3000 arbitrary response units (RUs), corresponding to 3 ng of the protein per flow cell (with the Biacore instrument calibrated at 1 RU ≈ 1 pg protein). The sensor chip was regenerated by stripping Ni^{2+} ions from the surface with a 3 min flush using NTA chip regeneration solution containing 350 mM EDTA after each series of binding analyses.

Covalent Immobilization of yCPR on CM5 Sensor Chip Surface. The yCPR was immobilized on a CM5 chip by covalent coupling *via* solvent-accessible protein lysine amino groups. For efficient covalent coupling, the protein was electrostatically concentrated near the dextran matrix. For this purpose a coupling solution with low ionic strength and pH lower than the protein isoelectric point has been used. The optimal pH value of 5.5 was experimentally determined for yCPR using the immobilization pH scouting protocol including injection of yCPR solutions at different pH values ranging from 7.4 through 5.0 over a sensor chip that has not been activated. The immobilization was carried out in four steps: (i) activation of carboxyl groups on the CM5 sensor surface, (ii) immobilization of yCPR, (iii) inactivation of residual active groups, and finally (iv) conditioning of the sensor surface with the running buffer (Figure 3, panel b). The surface of the CM5 chip was activated following a standard EDC/NHS amine coupling protocol. yCPR (0.65 μM in 10 mM acetate buffer, pH 5.5) was injected over an activated chip surface for 10 min followed by 10 min injection of HBS-EP running buffer to remove excess protein and then by 7 min injection of 1 M ethanolamine, pH 8.5, to inactivate residual active groups. Finally, the surface was washed with a 5 min pulse of HBS-EP buffer. Typically, about 12 ng of yCPR was immobilized per flow cell (12,000 RU), which is four times higher than the optimized yCPR immobilization level on Ni-NTA chip.

To avoid exposure of immobilized yCPR to the basic pH of the ethanolamine solution in control experiments, spontaneous inactivation of residual active groups in step (iii) was achieved by washing the chip surface with HBS-EP buffer continuously for several hours.

SPR-Based Binding Assays. All Biacore data were collected at 25 °C using a dual flow cell Biacore 3000 instrument (GE Healthcare) equipped with the Biacore Control and Evaluation Version 4.1 software. During the binding assays, the binding response signals in RUs were continuously recorded and presented graphically as a function of time. All the sensorgrams were processed by using Biacore Evaluation Version 4.1 software with

automatic correction for nonspecific bulk refractive index effect. The specific binding profiles of the compounds to the immobilized yCPR were obtained after subtracting the response signal from the control flow cell carrying no immobilized protein.

Probing CM5 Immobilized yCPR with the Organic Molecules. Each ligand binding cycle included four phases: (i) equilibration of the sensor surface carrying immobilized yCPR with the running buffer, (ii) association phase, consisting of 6 min injection of 25−35 μM compound solution in the running buffer at 10 μL min^{-1}, followed by (iii) compound dissociation upon 6 min injection of running buffer containing 3% DMSO, and finally (iv) surface regeneration with 1 M NaCl in the running buffer.

Steady-State Analysis of SPR Data. Steady-state binding experiments were carried out at different concentrations of FMN and FAD. The equilibrium signals (R_{eq}) were plotted against the ligand concentrations. The curve fitting efficiency was evaluated by χ^2 (average squared residual per data point (Table 1)), a statistical value in the Biacore technique. Under the conditions tested, the kinetics of flavin binding were fast enough to reach a plateau within the injection time, which allowed use of the steady-state R_{max} values to accurately calculate equilibrium constants. The blank run was subtracted from each sensorgram prior to data processing. The resulting sensorgrams were directly used for fitting. Data collected during the first 20 s after injection were excluded from the fitting procedure, as recommended by the manufacturer, to minimize sample dispersion and mass transport effects. Default software settings were kept for the fitting procedures.

To determine the equilibrium dissociation constant ($K_D = 1/K_A$) for the interaction, the equilibrium data were fitted to a single-site model:

$$R_{eq} = (R_{max} C K_A)/(1 + C K_A) \quad (1)$$

where R_{max} stands for the maximal response, C is the concentration of a ligand, R_{eq} is the equilibrium response at given ligand concentration, and K_A is the equilibrium association constant. All results are summarized in Table 1 as the average of five independent determinations.

Kinetic Analysis of SPR Data. Kinetic rate constants were calculated from the sensorgrams by globally fitting response curves obtained at various ligand concentrations to 1:1 binding model with baseline drift. Association (k_{on}) and dissociation (k_{off}) rate constants were fitted simultaneously:

$$\frac{dR}{dt} = k_{on} C(R_{max} - R) - k_{off} R \quad (2)$$

where R stands for the biosensor response of the formed complex, C is the concentration of the ligand, and R_{max} is the maximal theoretical value of binding response for a given ligand.

To compensate for a baseline drift, total biosensor response (R_{total}) for a complex is described by

$$R_{total} = R + R_I + D(t - t_{on}) \quad (3)$$

where R_I is a bulk refractive index contribution, D is a slope of the baseline drift, and t_{on} is the starting time for sample injection.

Equilibrium dissociation constants (K_D) were calculated as a ratio of the rate constants k_{off}/k_{on} and summarized in Table 1 as the average of five independent determinations.

Acknowledgment: We thank Dr. F. P. Guengerich for helpful discussions, Mr. Potter Wickware for critical reading of the manuscript, Ms. Larissa N. Skuratovskaya for valuable contributions. This work was supported by the National Institutes of Health RO1 grant GM078553 and by the Pilot/Feasibly grant P30 DK026743 from the UCSF Liver Center (to L.M.P.), and by the Russian Foundation for Basic Research grant 10-04-90026 (to A.S.I.).

REFERENCES

1. Laden, B. P., Tang, Y., and Porter, T. D. (2000) Cloning, heterologous expression, and enzymological characterization of human squalene monooxygenase, *Arch. Biochem. Biophys. 374*, 381–388.
2. Ono, T., and Bloch, K. (1975) Solubilization and partial characterization of rat liver squalene epoxidase, *J. Biol. Chem. 250*, 1571–1579.
3. Schacter, B. A., Nelson, E. B., Marver, H. S., and Masters, B. S. S. (1972) Immunochemical evidence for an association of heme oxygenase with the microsomal electron transport system, *J. Biol. Chem. 247*, 3601–3607.
4. Ilan, Z., Ilan, R., and Cinti, D. L. (1981) Evidence for a new physiological role of hepatic NADPH:ferricytochrome (P-450) oxidoreductase. Direct electron input to the microsomal fatty acid chain elongation system, *J. Biol. Chem. 256*, 10066–10072.
5. Enoch, H. G., and Strittmatter, P. (1979) Cytochrome b_5 reduction by NADPH-cytochrome P-450 reductase, *J. Biol. Chem. 254*, 8976–8981.
6. Narhi, L. O., and Fulco, A. J. (1986) Characterization of a catalytically self-sufficient 119,000-dalton cytochrome P-450 monooxygenase induced by barbiturates in *Bacillus megaterium*, *J. Biol. Chem. 261*, 7160–7169.
7. Gustafsson, M. C. U., Roitel, O., Marshall, K. R., Noble, M. A., Chapman, S. K., Pessegueiro, A., Fulco, A. J., Cheesman, M. R., Wachenfeldt, C., and Munro, A. W. (2004) Expression, purification, and characterization of *Bacillus subtilis* cytochromes P450 CYP102A2 and CYP102A3: flavocytochrome homologues of P450 BM3 from *Bacillus megaterium*, *Biochemistry 43*, 5474–5487.
8. Kitazume, T., Takaya, N., Nakayama, N., and Shoun, H. (2000) *Fusarium oxysporum* fatty-acid subterminal hydroxylase (CYP505) is a membrane-bound eukaryotic counterpart of *Bacillus megaterium* cytochrome P450BM3, *J. Biol. Chem. 275*, 39734–39740.
9. Bredt, D. S., Hwang, P. M., Glatt, C. E., Lowenstein, C., Reed, R. R., and Snyder, S. H. (1991) Cloned and expressed nitric oxide synthase structurally resembles cytochrome P-450 reductase, *Nature 351*, 714–718.
10. Leclerc, D., Wilson, A., Dumas, R., Gafuik, C., Song, D., Watkins, D., Heng, H. H. Q., Rommens, J. M., Scherer, S. W., Rosenblatt, D. S., and Gravel, R. A. (1998) Cloning and mapping of a cDNA for methionine synthase reductase, a flavoprotein defective in patients with homocystinuria, *Proc. Natl. Acad. Sci. U.S.A. 95*, 3059–3064.
11. Paine, M. J. I., Garner, A. P., Powell, D., Sibbald, J., Sales, M., Pratt, N., Smith, T., Tew, D. G., and Wolf, C. R. (2000) Cloning and characterization of a novel human dual flavin reductase, *J. Biol. Chem. 275*, 1471–1478.
12. Ostrowski, J., Barber, M. J., Rueger, D. C., Miller, B. E., Siegel, L. M., and Kredich, N. M. (1989) Characterization of the flavoprotein moieties of NADPH-sulfite reductase from *Salmonella typhimurium* and *Escherichia coli*. Physicochemical and catalytic properties, amino acid sequence deduced from DNA sequence of cysJ, and comparison with NADPH-cytochrome P-450 reductase, *J. Biol. Chem. 264*, 15796–15808.
13. Murataliev, M. B., Feyereisen, R., and Walker, F. A. (2004) Electron transfer by diflavin reductases, *Biochim. Biophys. Acta 1698*, 1–26.
14. Iyanagi, T. (2005) Structure and function of NADPH-cytochrome P450 reductase and nitric oxide synthase reductase domain, *Biochem. Biophys. Res. Commun. 338*, 520–528.

15. Masters, B. S. (2005) The journey from NADPH-cytochrome P450 oxidoreductase to nitric oxide synthases, *Biochem. Biophys. Res. Commun. 338*, 507–519.
16. Gutierrez, A., Grunau, A., Paine, M., Munro, A. W., Wolf, C. R., Roberts, G. C. K., and Scrutton, N. S. (2003) Electron transfer in human cytochrome P450 reductase, *Biochem. Soc. Trans. 31*, 497–501.
17. Aigrain, L., Pompon, D., Morera, S., and Truan, G. (2009) Structure of the open conformation of a functional chimeric NADPH cytochrome P450 reductase, *EMBO Rep 10*, 742–747.
18. Hamdane, D., Xia, C., Im, S. C., Zhang, H., Kim, J. J., and Waskell, L. (2009) Structure and function of an NADPH-cytochrome P450 oxidoreductase in an open conformation capable of reducing cytochrome P450, *J. Biol. Chem. 284*, 11374–11384.
19. Ellis, J., Gutierrez, A., Barsukov, I. L., Huang, W. C., Grossmann, J. G., and Roberts, G. C. (2009) Domain motion in cytochrome P450 reductase: conformational equilibria revealed by NMR and small-angle x-ray scattering, *J. Biol. Chem. 284*, 36628–36637.
20. Lamb, D. C., Kim, Y., Yermalitskaya, L. V., Yermalitsky, V. N., Lepesheva, G. I., Kelly, S. L., Waterman, M. R., and Podust, L. M. (2006) A second FMN binding site in yeast NADPH-cytochrome P450 reductase suggests a mechanism of electron transfer by diflavin reductases, *Structure 14*, 51–61.
21. Wang, M., Roberts, D. L., Paschke, R., Shea, T. M., Masters, B. S., and Kim, J. J. (1997) Three-dimensional structure of NADPH-cytochrome P450 reductase: prototype for FMN- and FAD-containing enzymes, *Proc. Natl. Acad. Sci. U.S.A. 94*, 8411–8416.
22. Nisimoto, Y. (1986) Localization of cytochrome *c*-binding domain on NADPH-cytochrome P-450 reductase, *J. Biol. Chem. 261*, 14232–14239.
23. Nisimoto, Y., and Otsuka-Murakami, H. (1988) Cytochrome b_5, cytochrome *c*, and cytochrome P-450 interactions with NADPH-cytochrome P-450 reductase in phospholipid vesicles, *Biochemistry 27*, 5869–5876.
24. Shen, A. L., and Kasper, C. B. (1995) Role of acidic residues in the interaction of NADPH-cytochrome P450 oxidoreductase with cytochrome P450 and cytochrome *c*, *J. Biol. Chem. 270*, 27475–27480.
25. Hubbard, P. A., Shen, A. L., Paschke, R., Kasper, C. B., and Kim, J. J. (2001) NADPH-cytochrome P450 oxidoreductase. Structural basis for hydride and electron transfer, *J. Biol. Chem. 276*, 29163–29170.
26. Vermilion, J. L., and Coon, M. J. (1978) Purified liver microsomal NADPH-cytochrome P-450 reductase. Spectral characterization of oxidation-reduction states, *J. Biol. Chem. 253*, 2694–2704.
27. Hayashi, S., Omata, Y., Sakamoto, H., Hara, T., and Noguchi, M. (2003) Purification and characterization of a soluble form of rat liver NADPH-cytochrome P-450 reductase highly expressed in *Escherichia coli*, *Protein Expression Purif. 29*, 1–7.
28. Nisimoto, Y., and Shibata, Y. (1982) Studies on FAD- and FMN-binding domains in NADPH-cytochrome P-450 reductase from rabbit liver microsomes, *J. Biol. Chem. 257*, 12532–12539.
29. Vermilion, J. L., and Coon, M. J. (1978) Identification of the high and low potential flavins of liver microsomal NADPH-cytochrome P-450 reductase, *J. Biol. Chem. 253*, 8812–8819.
30. Rich, R. L., and Myszka, D. G. (2000) Advances in surface plasmon resonance biosensor analysis, *Curr. Opin. Biotechnol. 11*, 54–61.
31. Vermilion, J. L., Ballou, D. P., Massey, V., and Coon, M. J. (1981) Separate roles for FMN and FAD in catalysis by liver microsomal NADPH-cytochrome P-450 reductase, *J. Biol. Chem. 256*, 266–277.
32. Khatua, A. K., and Bhattacharyya, M. (2001) NADPH-induced oxidative damage of rat liver microsomes: protective role of chlorpromazine and trifluoperazine, *Pol. J. Pharmacol. 53*, 629–634.
33. French, J. S., Guengerich, F. P., and Coon, M. J. (1980) Interactions of cytochrome P-450, NADPH-cytochrome P-450 reductase, phospholipid, and substrate in the reconstituted liver microsomal enzyme system, *J. Biol. Chem. 255*, 4112–4119.
34. Bonants, P. J., Muller, F., Vervoort, J., and Edmondson, D. E. (1990) A ^{31}P-nuclear-magnetic-resonance study of NADPH-cytochrome-P-450 reductase and of the *Azotobacter* flavodoxin/ferredoxin-NADP+ reductase complex, *Eur. J. Biochem. 190*, 531–537.
35. Narayanasami, R., Otvos, J. D., Kasper, C. B., Shen, A., Rajagopalan, J., McCabe, T. J., Okita, J. R., Hanahan, D. J., and Masters, B. S. (1992) ^{31}P NMR spectroscopic studies on purified, native and cloned, expressed forms of NADPH-cytochrome P450 reductase, *Biochemistry 31*, 4210–4218.
36. Balvers, W. G., Boersma, M. G., Vervoort, J., Ouwehand, A., and Rietjens, I. M. (1993) A specific interaction between NADPH-cytochrome reductase and phosphatidylserine and phosphatidylinositol, *Eur. J. Biochem. 218*, 1021–1029.
37. Muller-Enoch, D., Churchill, P., Fleischer, S., and Guengerich, F. P. (1984) Interaction of liver microsomal cytochrome P-450 and NADPH-cytochrome P-450 reductase in the presence and absence of lipid, *J. Biol. Chem. 259*, 8174–8182.
38. Auesukaree, C., Homma, T., Tochio, H., Shirakawa, M., Kaneko, Y., and Harashima, S. (2004) Intracellular phosphate serves as a signal for the regulation of the PHO pathway in *Saccharomyces cerevisiae*, *J. Biol. Chem. 279*, 17289–17294.
39. Entsch, B., Cole, L. J., and Ballou, D. P. (2005) Protein dynamics and electrostatics in the function of *p*-hydroxybenzoate hydroxylase, *Arch. Biochem. Biophys. 433*, 297–311.
40. Garcin, E. D., Bruns, C. M., Lloyd, S. J., Hosfield, D. J., Tiso, M., Gachhui, R., Stuehr, D. J., Tainer, J. A., and Getzoff, E. D. (2004) Structural basis for isozyme-specific regulation of electron transfer in nitric-oxide synthase, *J. Biol. Chem. 279*, 37918–37927.
41. Venkateswarlu, K., Lamb, D. C., Kelly, D. E., Manning, N. J., and Kelly, S. L. (1998) The N-terminal membrane domain of yeast NADPH-cytochrome P450 (CYP) oxidoreductase is not required for catalytic activity in sterol biosynthesis or in reconstitution of CYP activity, *J. Biol. Chem. 273*, 4492–6.
42. Humphrey, W., Dalke, A., and Schulten, K. (1996) VMD: visual molecular dynamics, *J. Mol. Graphics 14*, 33–38.
43. Pettersen, E. F., Goddard, T. D., Huang, C. C., Couch, G. S., Greenblatt, D. M., Meng, E. C., and Ferrin, T. E. (2004) UCSF Chimera—a visualization system for exploratory research and analysis, *J. Comput. Chem. 25*, 1605–1612.